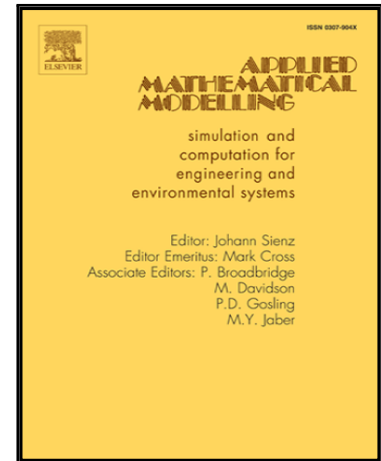


# Accepted Manuscript

Hybrid Flow Modelling Approach Applied to Automotive Catalysts

Sophie Porter, Jonathan Saul, Svetlana Aleksandrova,  
Humberto Medina, Stephen Benjamin

PII: S0307-904X(16)30225-6  
DOI: [10.1016/j.apm.2016.04.024](https://doi.org/10.1016/j.apm.2016.04.024)  
Reference: APM 11145



To appear in: *Applied Mathematical Modelling*

Received date: 9 November 2015  
Revised date: 17 April 2016  
Accepted date: 26 April 2016

Please cite this article as: Sophie Porter, Jonathan Saul, Svetlana Aleksandrova, Humberto Medina, Stephen Benjamin, Hybrid Flow Modelling Approach Applied to Automotive Catalysts, *Applied Mathematical Modelling* (2016), doi: [10.1016/j.apm.2016.04.024](https://doi.org/10.1016/j.apm.2016.04.024)

This is a PDF file of an unedited manuscript that has been accepted for publication. As a service to our customers we are providing this early version of the manuscript. The manuscript will undergo copyediting, typesetting, and review of the resulting proof before it is published in its final form. Please note that during the production process errors may be discovered which could affect the content, and all legal disclaimers that apply to the journal pertain.

**Highlight**

- A novel hybrid approach is proposed for modelling a catalyst monolith.
- The model combines individual channels with a porous region downstream.
- Predictions retain accuracy of individual channels model.
- Computational demand is reduced compared to individual channels.
- The model provides a good compromise between the two approaches.

ACCEPTED MANUSCRIPT

# Hybrid Flow Modelling Approach Applied to Automotive Catalysts

Sophie Porter\*, Jonathan Saul, Svetlana Aleksandrova, Humberto Medina, Stephen Benjamin

*Faculty of Engineering and Computing, Coventry University, UK*

---

## Abstract

Catalytic converters are employed in automotive emissions aftertreatment for the reduction of pollutants. Flow behaviour in a catalyst system may be modelled using computational fluid dynamics. This study concerns a planar catalytic converter system with a wide-angled planar diffuser under steady flow conditions, in which the flow is approximately two-dimensional. The catalyst monolith is modelled using a novel hybrid approach. Individual channels at the entrance to the substrate provide an accurate description of flow upon entrance to the monolith. A porous region then applies the macroscopic pressure drop on the fully developed flow. Flow predictions are compared with experimental data in the diffuser and downstream of the monolith. Overall, the hybrid model improves upon the separate use of the two approaches. The variance of downstream velocity predictions from experimental data is decreased by up to 50% compared to the porous medium model, whilst the computational demand is reduced by approximately one order of magnitude compared to the individual channels model.

*Keywords:* automotive catalyst, modelling, oblique entry

---

## 1. Introduction

Catalytic converters are employed in the automotive industry for compliance with emissions regulations. The catalyst is commonly a monolith comprised of many parallel channels of small hydraulic diameter ( $\sim 1$  mm). A washcoat applied to the channel walls is deposited with precious metals, creating a large surface area for the reaction of exhaust gases. A wide-angled diffuser connects the exhaust pipe to the front face of the catalyst, resulting in flow separation in the diffuser and non-uniformly distributed flow in the catalyst, as shown in Figure 1.

Non-uniform flow entering the catalyst affects its conversion efficiency [1–3], degradation rate [2] and light-off performance [4]. The level of flow maldistribution is a key factor in the design process of catalytic converters and is commonly used in the automotive industry. A relatively simple measure

---

\*Corresponding author

*Email address:* porters5@coventry.ac.uk (Sophie Porter)

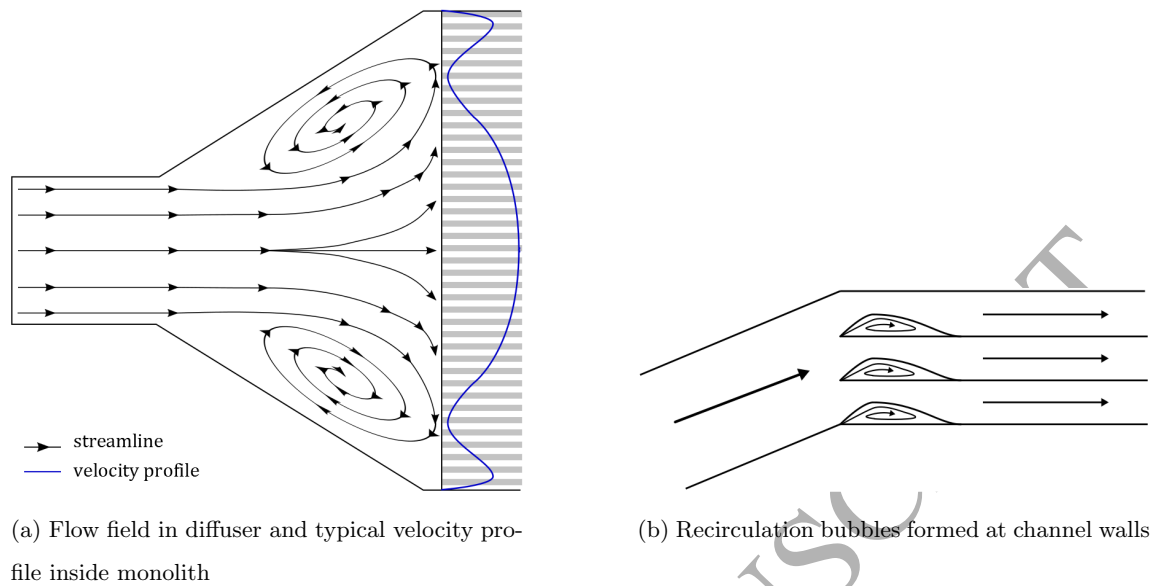


Figure 1: Example of flow behaviour in a catalytic converter system

of conversion efficiency can then be obtained for post light-off conditions where reactions are mass-transfer limited [3, 5, 6]. Conversion efficiency  $\eta$  as a function of flow velocity can then be described by Eq. 1 [5]:

$$\eta = 1 - \exp\left(\frac{-4Lk_c}{u_c d_h}\right) \quad (1)$$

where  $L$  is the length of the monolith channel,  $u_c$  is the channel velocity,  $d_h$  is the channel hydraulic diameter, and  $k_c$  is the mass transfer coefficient which may be determined theoretically [7]. Such an expression may then be readily integrated across the predicted velocity profile to obtain an estimation of overall conversion efficiency. An example of this is found in the work of Karvounis and Assanis [3], who considered the global mass transfer through the monolith and were thereby able to analyse the effect of non-uniformly distributed flow on the conversion efficiency of a catalytic converter.

As may be seen in Figure 1(a), flow separates at the diffuser inlet and a confined jet traverses the diffuser. High axial resistance causes the flow to spread radially at the monolith face, with some flow entering the channels. Away from the centre, flow enters the channels obliquely or feeds into recirculation regions between the jet and the diffuser wall. Oblique flow at the monolith face results in separation at the channel entry, as presented in Figure 1(b). There is a build-up of pressure in the region where the diffuser wall connects to the monolith, and flow is forced into the outermost channels. This results in the secondary maxima of the characteristic saddle-shaped velocity profile, illustrated in Figure 1(a).

Computational fluid dynamics (CFD) provides an alternative to measurement techniques for the

assessment of flow maldistribution and initial evaluation of designs prior to reaction modelling. Resolving the entire fluid domain incurs high computational demand [8], however this may be overcome by considering the macroscopic effect of the monolith on the flow field by representing the monolith as an equivalent continuum, as described in detail in [9]. The associated axial pressure drop is often derived from theoretical formulations, e.g. [4, 10], or defined from empirical results, assuming one-directional flow. However, this assumption is an over-simplification [11] and additional pressure losses due to oblique entry have been found to be non-negligible [12, 13]. The effect of oblique entry on pressure loss may be approximated by the expression derived by Küchemann and Weber [14]:

$$\Delta P_{\text{obl}} = \frac{\rho v^2}{2} \quad (2)$$

where  $v$  is the transverse velocity at the monolith face.

Benjamin et al. [15] found that accounting for pressure losses due to oblique entry using Eq. 2 increased the predicted flow non-uniformity, improving maximum velocity predictions but over-predicting the magnitude of secondary peaks. This may be due to an overcompensation of pressure losses at areas of high angle of attack. Quadri et al. [12] therefore proposed an expression for pressure drop dependent on a *critical angle*, where oblique pressure losses are assumed constant for flow at a specified entry angle and above. Indeed, Porter et al. [8] found that a *critical angle* of  $69^\circ$  resulted in the most consistent level of agreement with experimental data across the range of cases considered. It is precisely this complex dynamic of flow entering the monolith and its effect on the profile downstream that promotes modelling the monolith channels individually.

Porter et al. [8] modelled the monolith as individual channels and found overall improvement in the agreement of flow maldistribution predictions with experimental data compared to the porous medium model, particularly for the longer monolith case which presents higher overall resistance. The mesh is refined in the channels and is thus able to capture flow behaviour upon entrance into the monolith. Recirculation bubbles are apparent at the channel walls and the developing boundary layer along each channel is well-defined. Comparing velocity profiles in the diffuser, it is surmised that the method for modelling the channels has little influence upstream, except for the flow immediately upstream of the monolith face [8].

The current study aims to combine the porous medium and individual channels methods for modelling the monolith in order to develop an accurate but computationally practical model. Individual channels at the front of the monolith resolve the effect of obliqueness on the flow and a porous region is employed for fully developed flow downstream. It is hypothesised that the model will economise on the individual channels model whilst retaining accuracy.

## 2. Methodology

This study presents the application of CFD to modelling flow in a catalytic converter system with a planar diffuser. Two monoliths with identical cell geometry are used, with lengths 27 mm and 100 mm. Test case parameters are listed in Table 1.

Reynolds numbers (Re) are based on the uniform inlet velocity and hydraulic diameter of the nozzle and were chosen to be representative of typical passenger sized vehicles. For example,  $Re = 2.2 \times 10^4$  corresponds to the engine speed at which peak torque occurs for a typical 2 L 4-cylinder internal combustion engine. Also given in Table 1 are the values of space velocity ( $GHSV$ ), a measure denoting the ratio of the hourly volumetric feed-gas flow rate to the reactor (catalyst bed) volume.

Table 1: Test cases

Re	$L$ (mm)	$GHSV$ ( $h^{-1}$ )
$2.2 \times 10^4$	27	$3.6 \times 10^5$
$2.2 \times 10^4$	100	$9.7 \times 10^4$
$3.0 \times 10^4$	27	$5.4 \times 10^5$
$3.0 \times 10^4$	100	$1.5 \times 10^5$
$4.2 \times 10^4$	27	$7.2 \times 10^5$
$4.2 \times 10^4$	100	$1.9 \times 10^5$

### 2.1. Experimental Data Collection

Flow measurements were taken on a two-dimensional isothermal flow rig with a planar diffuser. A schematic diagram is given in Figure 2; the set-up is presented by Mat Yamin et al. [16] and is summarised here.

Air is supplied via a viscous flow meter (1) to a plenum (2) with flow straightener (3) and axisymmetric nozzle (4). Steady state measurements for the current study were obtained by fixing the rotor of the pulse generator (5) in a fully open position. Air flows through a flow straightener (6) and past a resonator box (7), installed to shape pulses during pulsating flow studies. A particle generator (9) supplies seeding to a second plenum (8) with a flow straightener (10) to minimise any swirl components. A two-dimensional nozzle (11) provides uniform flow to the planar diffuser (12). The diffuser has inlet dimensions  $24 \times 96$  mm, outlet dimensions  $78 \times 96$  mm, length 48 mm and total included angle of approximately  $60^\circ$ . The diffuser is made of crown glass for optimal optical conditions for PIV. The diffuser outlet attaches to an unwashcoated cordierite monolith (13) with channel hydraulic diameter 1.12 mm, a nominal cell density of 62 cells/cm<sup>2</sup> and porosity 0.77. An outlet sleeve (14) 50 mm long minimised any influence from air outside the rig. Two sleeves were used: A fitted sleeve of dimensions

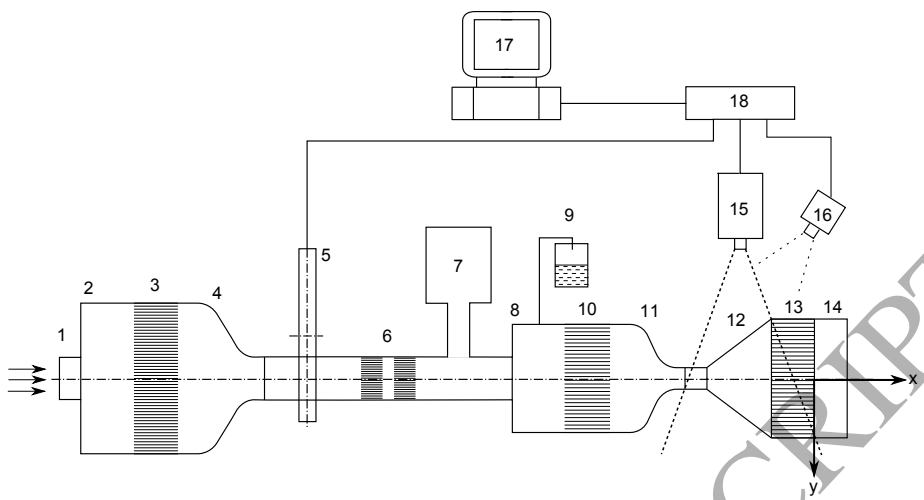


Figure 2: Schematic of flow rig

78 × 96 mm for downstream hot-wire anemometry (HWA) measurements and an expanded sleeve of dimensions 125 × 96 mm during particle image velocimetry (PIV) data collection in the diffuser.

Flow within the diffuser was measured using a TSI PIV system. A six-jet atomiser at 25 psi produced olive oil droplets of approximately 0.6 μm diameter. A cylindrical lens of -25 mm focal length was combined with a spherical lens of 500 mm to transform the circular beam from a 120 mJ solid-state Nd:YAG laser into an approximately 1 mm thick light sheet at a stand-off distance of 0.5 m to illuminate the seeded flow. A 4-megapixel CCD camera with 2048 × 2048 pixel (1 pixel = 7.4 μm) resolution was used to capture the flow field. The camera, coupled with a 105 mm lens, was placed 0.8 m from the measurement plane to cover an 80 × 60 mm field of view, resulting in a magnification factor of 0.155. An f-number of 11 enabled a particle image diameter above 2 pixels, avoiding pixel locking. INSIGHT-3G software, using the recursive Nyquist method with a 64 × 64 initial grid and a final grid of 32 × 32 pixels, yielded 95% valid vectors in each field and a vector resolution of 0.76 mm.

Axial velocity profiles at the nozzle exit and 40 mm downstream of the monolith were obtained using a TSI IFA 300 HWA system. 5 μm platinum-plated tungsten wires (Dantec 55 P11) were calibrated on an automatic TSI 1129 calibration rig. A 1 MHz 4 channel 12 bit A/D converter converted the IFA output voltage (within ±5 V) to a digital signal to be processed by ThermalPro software. HWA measurement is subject to an uncertainty of ±1% [17].

## 2.2. Numerical Model

Flow predictions were obtained using the commercial CFD solver STAR-CCM+. Flow in the system has been found to be two-dimensional and symmetrical [16]. It is therefore sufficient for the flow domain to consist of half-widths of the diffuser, monolith and outlet sleeve. Figure 3 shows the

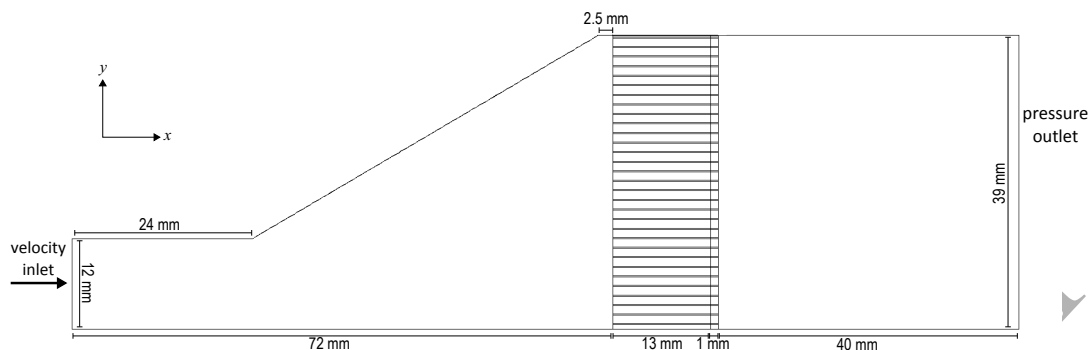
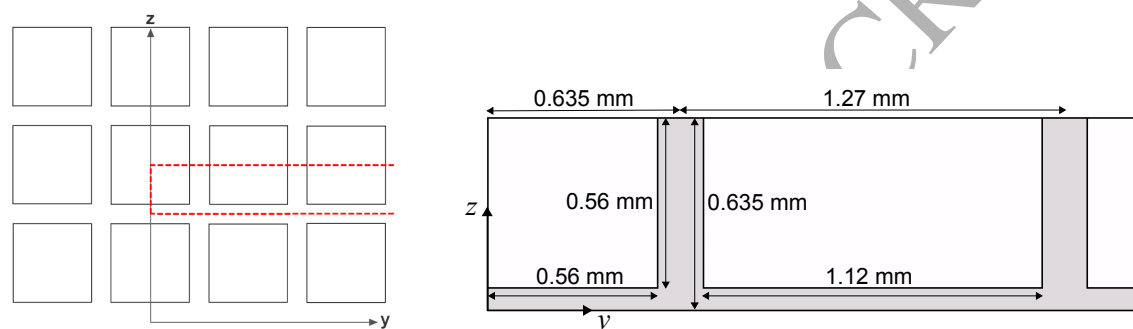


Figure 3: Geometry schematic



(a) Section of monolith modelled as channels

(b) Dimensions of channels

Figure 4: Schematic showing (a) derivation and (b) geometry of channels section

geometry of the modelled flow domain, with the monolith modelled as a combination of channels of length 13 mm and a porous medium of length 1 mm.

Individual channels at the entrance to the monolith are able to accurately capture the effects of the flow behaviour immediately upstream of the monolith face. Flow in the channels is assumed to be symmetric about the channel half-height ( $z$  direction). For symmetry, the first cell lies on the centre-line and thus only half its width ( $y$  direction) is included. Full cell widths are then included for full coverage of the diffuser outlet and individual channels are located between solid walls. Figure 4(a) shows the channels geometry (marked by --) as a portion of the monolith cross-section. The channels have hydraulic diameter 1.12 mm and a nominal cell density of 62 cells/cm<sup>2</sup>. A portion of the cross-sectional geometry of the channels is shown in Figure 4(b).

As shown in Figure 3, the individual channels have length 13 mm, sufficient to capture the effects of oblique entry. A 1 mm porous section downstream of the channels implements the overall pressure drop of the fully-developed flow, that is, the 1 mm section represents 14 mm and 87 mm respectively

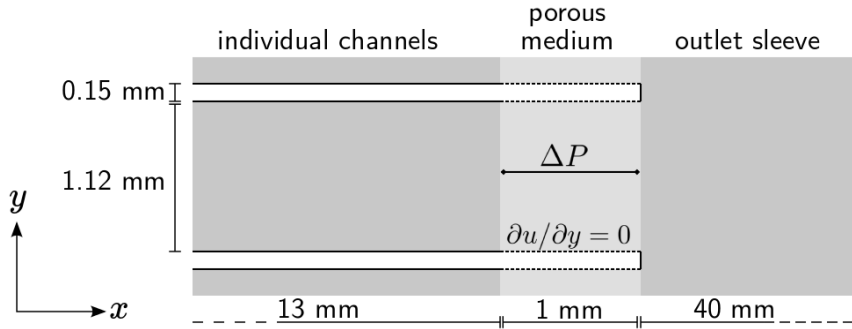


Figure 5: Computational model schematic of one channel end section

for the 27 mm and 100 mm monoliths. Figure 5 shows the downstream portion of the monolith at the interface with the outlet sleeve. Porous sections have slip walls, i.e. shear stress  $\tau = \mu \partial u / \partial y = 0$ , where  $u$  and  $y$  denote the velocity of the fluid along the boundary and the distance from the boundary respectively.

The axial resistance coefficient for the porous section is derived using the Hagen-Poiseuille equation for fully-developed laminar channel flow,  $\Delta P^* = (fRe_c)(4X^+)$ , giving a linear relationship between the pressure drop per unit length and channel velocity:

$$\frac{\Delta P}{L} = \frac{2(fRe_c)\mu}{d_h^2} u_c \quad (3)$$

where  $fRe_c = 14.227$  for a square cross-section. Eq. 3 is implemented in the model as the axial component of the porous source term  $\mathbf{f}_P$  in the momentum equations, where

$$\mathbf{f}_P = -(\mathbf{P}_v + \mathbf{P}_i|\mathbf{v}|) \cdot \mathbf{v} \quad (4)$$

and  $\mathbf{P}_v$  and  $\mathbf{P}_i$  denote the viscous and inertial resistance tensors respectively [18]. Since the Hagen-Poiseuille equation assumes fully-developed flow, the viscous effects of the flow dominate and  $\mathbf{P}_i$  has zero magnitude.

Reynolds averaged Navier-Stokes (RANS) equations are combined with the  $v^2f$  turbulence model. As well as solving transport equations for turbulent kinetic energy and dissipation rate, the normal stress function ( $v^2$ ) and the elliptic function ( $f$ ) are resolved, improving accuracy for near-wall turbulence effects and thus flow separation compared to other eddy viscosity models [19]. The level of separation in the diffuser and in the entrance of monolith channels (Figure 1) makes the  $v^2f$  model a suitable approach to the system considered in this work.

Near-wall turbulence modelling in Star-CCM+ is derived from equilibrium turbulent boundary layer theory for  $y^+ > 30$ , however the viscous sublayer is assumed resolved for lower values of  $y^+$  and wall laws are not incorporated [18].

Flow in the downstream region of the monolith channels is laminar. Since these regions are modelled as a porous medium in the simulation, turbulent velocity fluctuations are not considered and it is therefore justifiable to apply the same turbulence modelling equations across the entire model.

Velocity and turbulence properties are uniform at the diffuser inlet and the values of turbulence intensity, 0.01, and viscosity ratio, 10, are specified at the inlet. The model is meshed on a regular hexahedral grid with refinement at the channels. Prism layers are included at all wall boundaries to capture the developing boundary layer and  $y^+ \leq 1$  was obtained.

Computational demand may be demonstrated by the number of cells,  $N$ , required for a mesh-independent model. Table 2 compares the computational resources used in [8] and in the current study. Compared to the individual channels model, the current hybrid model greatly reduces the number of cells required and has the benefit of being independent of monolith length.

Table 2: Number of cells used for each model

Model	$N$	
	$L = 27$ mm	$L = 100$ mm
porous medium	$2.8 \times 10^4$	$4.7 \times 10^4$
individual channels	$4.0 \times 10^6$	$8.8 \times 10^6$
hybrid	$9.1 \times 10^5$	$9.1 \times 10^5$

### 3. Results & Analysis

Figure 6 shows normalised velocity contours on the symmetry plane of the model for the case of a 27 mm monolith with  $Re = 4.2 \times 10^4$ . At the expansion of the diffuser, flow separates and a jet traverses the diffuser. The resistance presented by the channels forces the flow to spread radially immediately upstream of the monolith face. Flow enters the channels obliquely away from the diffuser centre, causing recirculation bubbles to form at the channel walls, as can be seen in the enlargement of the entrance into a channel shown in Figure 6. As the flow progresses along the channel, a boundary layer develops and the velocity profile becomes increasingly parabolic. The high axial viscous resistance of the porous region opposes the channel flow. The profile is flattened, however jets exiting the monolith remain distinguishable in the sleeve. Jets are less visible as more spreading occurs downstream, resulting in a relatively smooth velocity profile at the outlet.

Flow distribution in the catalyst is largely dependent on the interaction between the flow and the monolith face. Accurate model predictions in this critical region are therefore highly important. Figure 7 compares predicted velocities in the diffuser with PIV measurements for the case with inlet  $Re = 4.2 \times 10^4$ ,  $L = 27$  mm. Figure 7(a) shows profiles taken at a cross-section 2.5 mm upstream

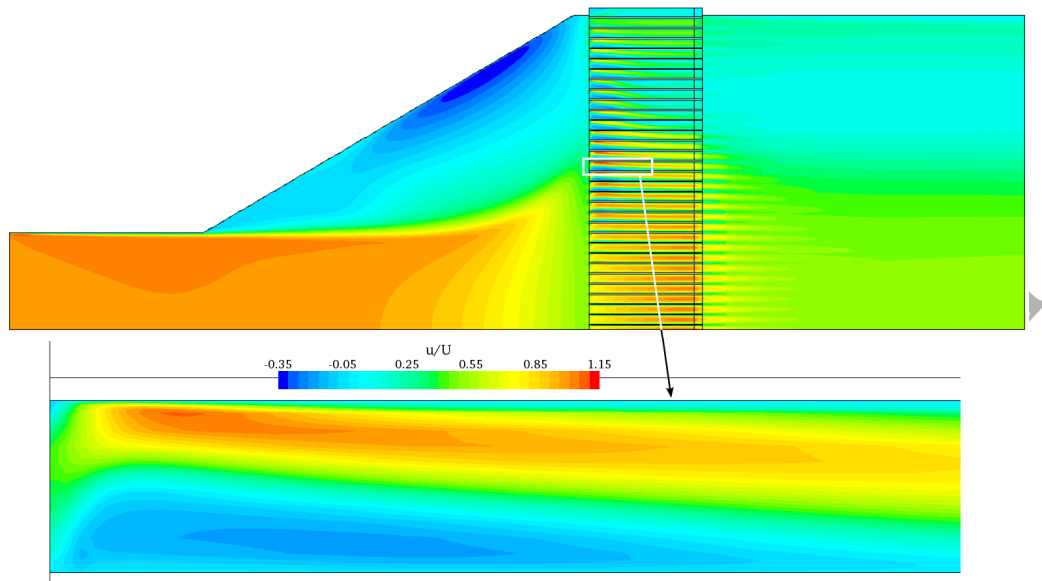


Figure 6: Axial velocity contours for  $L = 27$  mm,  $Re = 4.2 \times 10^4$

of the monolith, the closest measurement obtained [17]. Velocity predictions from the hybrid model are compared with predictions for the identical case from the porous medium and individual channels models presented in [8]. The porous medium model simulates the pressure drop across the monolith by representing the entire length as a porous region with porous resistance tensors derived from experimental measurements, and an entrance effect defined by Eq. 2. The individual channels model resolves the entire flow field in the  $x$  and  $y$  directions, assuming periodicity in the  $z$  direction.

At such close proximity to the monolith, the method of modelling the monolith resistance affects the upstream velocity. Predictions from the hybrid model fall between those from the two separate approaches. Axial velocities show a slight over-prediction of the central jet width and tangential velocities show over-predicted obliqueness outside of the central region, corresponding to a high level of shear at the edge of the spreading core, as seen in Figure 7(b).

Figure 8 presents axial velocity profiles 40 mm downstream of the monolith. CFD predictions from the study are compared with experimental HWA measurements and the porous medium and individual channels CFD approaches presented in [8], with velocities normalised by the mean downstream velocity.

HWA measurements were taken across the full width of the outlet sleeve. The velocity profiles denoted by ‘HWA 1’ and ‘HWA 2’ in Figure 8 show measurements either side of the symmetry plane of the system, and variability between the two measurements is observable. Similar variability of around  $\pm 5\%$  was observed by Mat Yamin [17].

As found in [15], the application of a porous medium model with an oblique entry effect predicts

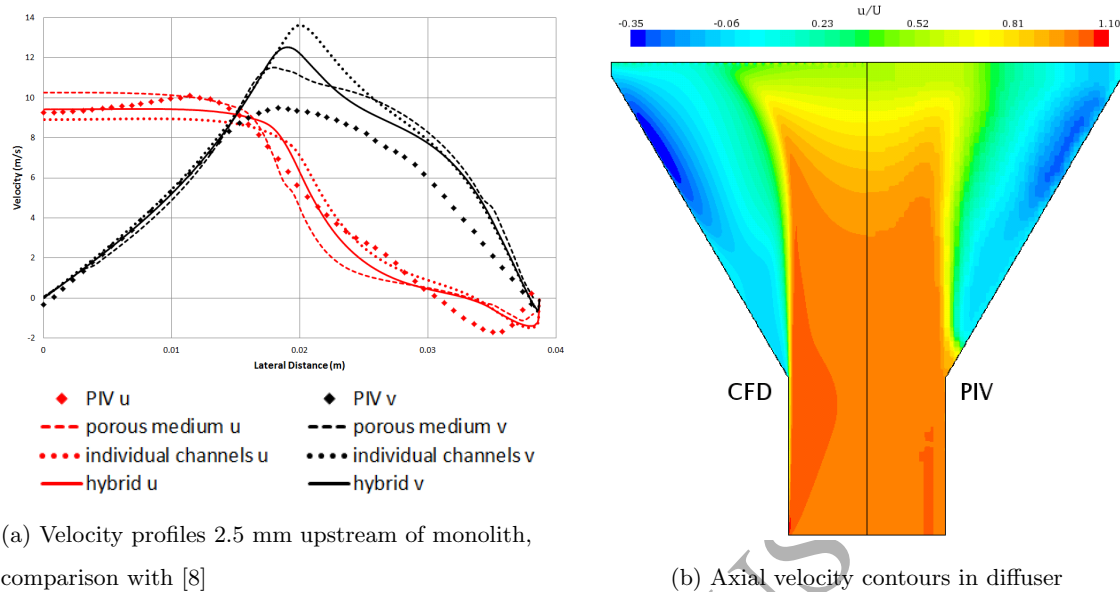


Figure 7: Velocity in diffuser for  $L = 27$  mm,  $Re = 4.2 \times 10^4$

much higher flow maldistribution than measured experimentally. At areas of high angle of attack, Eq. 2 produces a high pressure drop, resulting in low velocities at these locations downstream in the monolith and a more maldistributed flow profile. Velocity profiles from the individual channels model are more uniform than experimental results, but show more consistent agreement across monolith lengths compared to the porous medium model.

Velocity profiles predicted by the hybrid model are highly similar to those from the individual channels model, demonstrating the importance of accurately capturing flow behaviour at the entry to the monolith. The effect of combining this model with a porous section is most visible near to the sleeve wall. Flow maldistribution is increased compared to the individual channels model. Particularly present for the short monolith higher  $Re$  case shown in Figure 8(c), maxima at the centre and near the wall are higher and velocity at the trough is lower, showing improved agreement with experimental data. Profile predictions for the longer monolith are fairly uniform, with the hybrid model showing improvement compared to the individual channels model near to the wall. This may be attributed to the differences in flow behaviour upstream (Figure 7(a)) which in turn arise from the difference in pressure losses across the monolith. Improvement may also be linked to the turbulence modelling approach applied in the region of fully-developed flow in the monolith. Profiles are noticeably unsmooth, with the jet from each channel remaining identifiable downstream, particularly for the high  $Re$  case shown in Figure 8(f).

The level of agreement between CFD predictions and experimental measurements may be defined

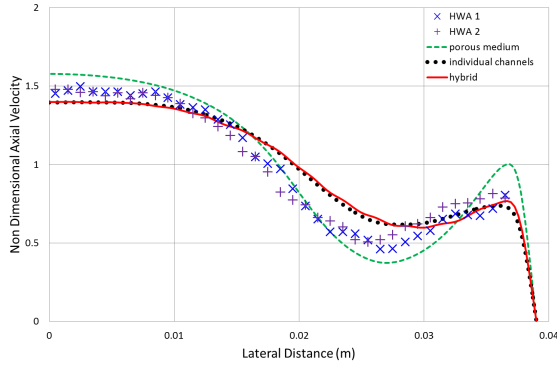
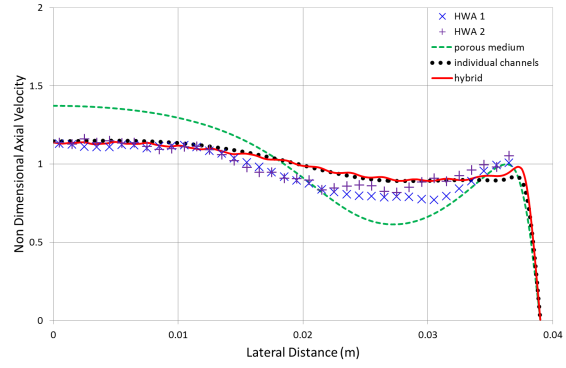
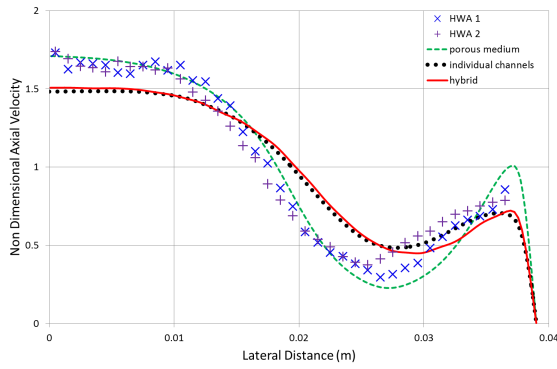
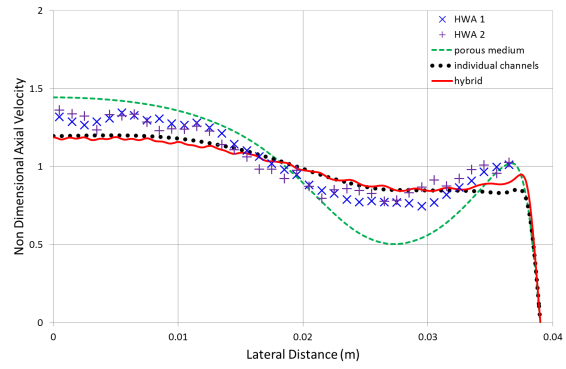
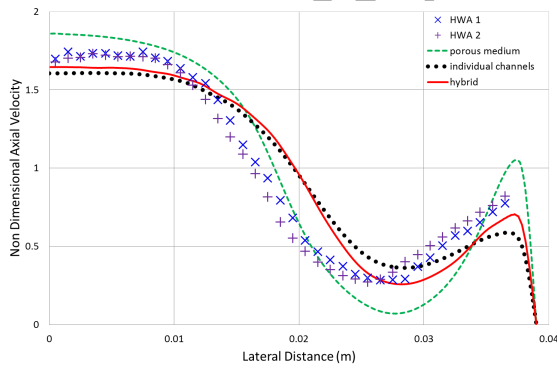
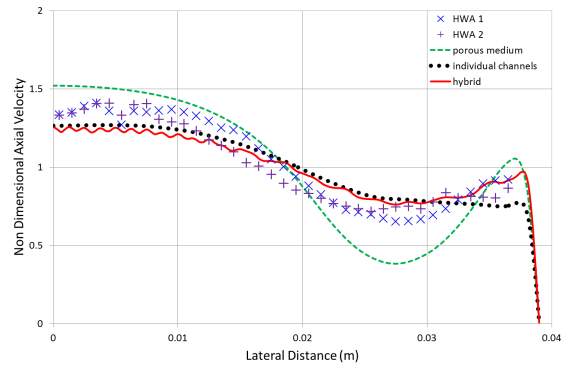
(a)  $L = 27$  mm,  $Re = 2.2 \times 10^4$ (d)  $L = 100$  mm,  $Re = 2.2 \times 10^4$ (b)  $L = 27$  mm,  $Re = 3.0 \times 10^4$ (e)  $L = 100$  mm,  $Re = 3.0 \times 10^4$ (c)  $L = 27$  mm,  $Re = 4.2 \times 10^4$ (f)  $L = 100$  mm,  $Re = 4.2 \times 10^4$ 

Figure 8: Axial velocity profiles 40 mm downstream of the monolith

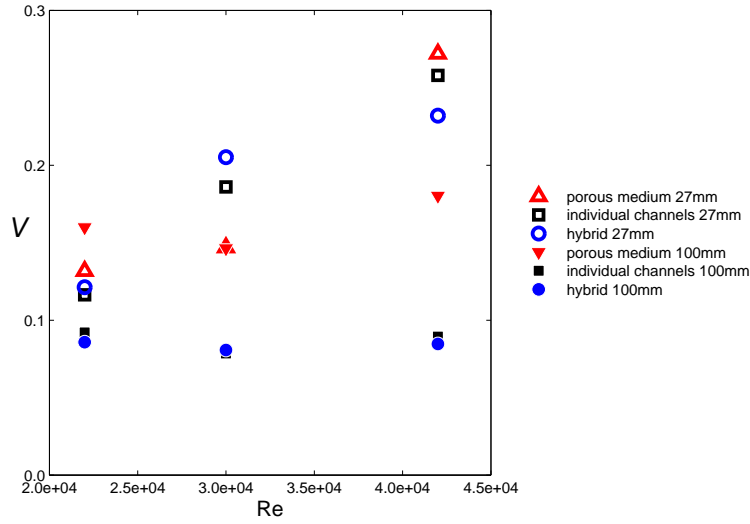


Figure 9: Variance

by the variance of model predictions from HWA data points, as presented in Figure 9. For each CFD approach, the predicted velocity profile is interpolated to the spatial coordinates of the experimental data and the mean difference in velocity, normalised by the HWA velocity, is calculated:

$$V = \frac{1}{n} \sum_{i=1}^n \frac{|\hat{u}_i - u_i|}{u_i} \quad (5)$$

where  $u_i$  denotes the velocities measured by HWA,  $\hat{u}_i$  denotes the interpolated velocity values for each model, an  $n$  is the total number of HWA data points.

Comparing the mean variance across velocity profiles, Figure 9 shows the hybrid model to provide limited improvement on the individual channels model. The higher Reynolds number, short monolith case shown in Figure 8(c) sees the greatest reduction in variance,  $\sim 10\%$ .

Figure 10 compares the non-uniformity index  $\psi$  from the model predictions and the experimental data. The non-uniformity index is defined as

$$\psi = \frac{\sigma}{U} \quad (6)$$

and is calculated using the mass flow weighted velocity over the monolith face.  $\sigma$  is defined as

$$\sigma = \frac{1}{\dot{m}} \int_A |u_i - U| \delta \dot{m} \quad (7)$$

which is equivalent to

$$\sigma = \frac{1}{n} \sum_{i=1}^n |u_i - U| u_i \quad (8)$$

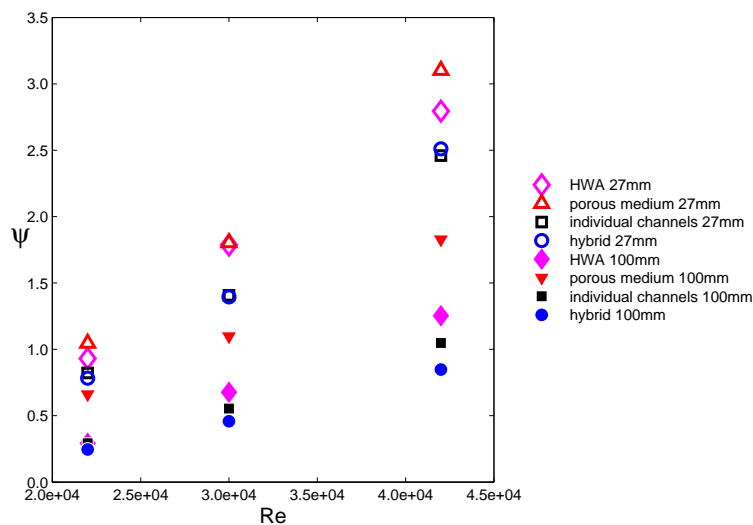


Figure 10: Non-uniformity index

for a velocity profile of discrete data, where  $u_i$  and  $U$  respectively denote the local axial velocity and the mean axial velocity. Non-uniformity values of experimental data are approximately equidistant to the predicted values from CFD for the shorter monolith. However for the longer monolith case, the porous medium model performs markedly worse in the prediction of flow maldistribution than the other models. Figure 10 shows simulations exhibiting the same trend as experiment, with the maldistribution index increasing with  $Re$  and as monolith resistance is reduced. This is consistent with studies for axisymmetric assemblies, e.g. [11]. For the important case where maldistribution is greatest,  $Re = 4.2 \times 10^4$  and 27 mm monolith, it is encouraging to note that hybrid model predictions are within 10% of experiment.

Discrepancies between hybrid model predictions and experimental data may be due to assumptions in the model. The geometry for the channels is derived from the manufacturer's specifications, however this assumes uniformity throughout the monolith. In reality, channel inlets at the monolith face are not identical and channel lengths are not perfectly straight. Roughness of the channel walls is neglected, possibly affecting the accuracy of boundary layer prediction within the channels.

#### 4. Conclusion

A CFD model combining individual channels and a porous medium to simulate flow behaviour in an automotive catalyst system has been developed and compared with experimental measurements upstream and downstream of the monolith. Predictions from the hybrid method show good agreement with experimental data, with predictions within 10% for the longer monolith case, providing a

compromise between the computational efficiency of the porous medium model and the geometrical accuracy of individual channels. Compared to individual channels, the hybrid model retains consistent agreement across the Reynolds number range and the two lengths of monolith, with improved agreement at secondary maxima locations. Computational demand is reduced by approximately one order of magnitude for the quasi-two-dimensional case, signifying the potential for high efficiency of computational cost in similar systems modelled in three dimensions. By considering the predicted velocity profile at the monolith front face and associated mass transfer, the model may also be extended to chemically reacting flows for post light-off conditions.

## References

- [1] A. P. Martin, N. S. Will, A. Bordet, P. Cornet, C. Gondoin, X. Mouton, Effect of flow distribution on emissions performance of catalytic converters, SAE Technical Paper 980936. doi:10.4271/980936.
- [2] J. S. Howitt, T. C. Sekella, Flow effects in monolithic honeycomb automotive catalytic converters, SAE Technical Paper 740244. doi:10.4271/740244.
- [3] E. Karvounis, D. N. Assanis, The effect of inlet flow distribution on catalytic conversion efficiency, *Int. J. Heat Mass Transfer* 36 (6) (1993) 1495–1504.
- [4] K. Zygourakis, Transient operation of monolith catalytic converters: a two-dimensional reactor model and the effects of radially nonuniform flow distributions, *Chemical Engineering Science* 44 (9) (1989) 2075–2086. doi:10.1016/0009-2509(89)85143-7.
- [5] S. F. Benjamin, Z. Liu, C. A. Roberts, Automotive catalyst design for uniform conversion efficiency, *Applied Mathematical Modelling* 28 (6) (2004) 559–572. doi:10.1016/j.apm.2003.10.008.
- [6] S.-J. Jeong, W. S. Kim, A three-dimensional numerical study of the effect of pulsating flow on conversion efficiency inside a catalytic converter, *Proceedings of the Institution of Mechanical Engineers, Part D: Journal of Automobile Engineering* 215 (1) (2001) 45–61. doi:10.1243/0954407011525458.
- [7] M. Bhattacharya, M. P. Harold, V. Balakotaiah, Mass-transfer coefficients in washcoated monoliths, *AIChE Journal* 50 (11) (2004) 2939–2955. doi:10.1002/aic.10212.
- [8] S. J. Porter, A. K. Mat Yamin, S. Aleksandrova, S. F. Benjamin, C. A. Roberts, J. M. Saul, An assessment of CFD applied to steady flow in a planar diffuser upstream of an automotive catalyst monolith, *SAE International Journal of Engines* 7 (4). doi:10.4271/2014-01-2588.

- [9] S. F. Benjamin, C. A. Roberts, Modelling warm-up of an automotive catalyst substrate using the equivalent continuum approach, *International Journal of Vehicle Design* 22 (3/4) (1999) 253–273. doi:10.1504/IJVD.1999.001868.
- [10] C. Ozhan, D. Fuster, P. Da Costa, Multi-scale flow simulation of automotive catalytic converters, *Chemical Engineering Science* 116 (2014) 161–171. doi:10.1016/j.ces.2014.04.044.
- [11] S. F. Benjamin, R. J. Clarkson, N. Haimad, N. S. Girgis, An experimental and predictive study of the flow field in axisymmetric automotive exhaust catalyst systems, SAE Technical Paper 961208. doi:10.4271/961208.
- [12] S. S. Quadri, S. F. Benjamin, C. A. Roberts, An experimental investigation of oblique entry pressure losses in automotive catalytic converters, *Proceedings of the Institution of Mechanical Engineers, Part C: Journal of Mechanical Engineering Science* 223 (11) (2009) 2561–2569. doi:10.1243/09544062JMES1565.
- [13] T. Persoons, M. Vanierschot, E. Van den Bulck, Oblique inlet pressure loss for swirling flow entering a catalyst substrate, *Experimental Thermal and Fluid Science* 32 (6) (2008) 1222–1231. doi:10.1016/j.expthermflusci.2008.02.002.
- [14] D. Küchemann, J. Weber, *Aerodynamics of propulsion*, McGraw-Hill, New York, 1953.
- [15] S. F. Benjamin, N. Haimad, C. A. Roberts, J. Wollin, Modelling the flow distribution through automotive catalytic converters, *Proceedings of the Institution of Mechanical Engineers, Part C: Journal of Mechanical Engineering Science* 215 (4) (2001) 379–383. doi:10.1243/0954406011520779.
- [16] A. K. Mat Yamin, S. F. Benjamin, C. A. Roberts, Pulsating flow in a planar diffuser upstream of automotive catalyst monoliths, *International Journal of Heat and Fluid Flow* 40 (2013) 43–53. doi:10.1016/j.ijheatfluidflow.2013.01.014.
- [17] A. K. Mat Yamin, Pulsating flow studies in a planar wide-angled diffuser upstream of automotive catalyst monoliths, Ph.D. thesis, Coventry University (2012).
- [18] CD-adapco, Star-CCM+ Version 8.04 User Guide (2013).
- [19] D. Cokljat, S. E. Kim, G. Iaccarino, P. A. Durbin, A comparative assessment of the V2F model for recirculating flows, in: 41st Aerospace Sciences Meeting and Exhibit, Reno, Nevada, 2003. doi:AIAA-2003-675.

## Notation

$\Delta P$	axial pressure drop
$\Delta P^*$	non-dimensional axial pressure drop, $\Delta P / \frac{1}{2} \rho u_c^2$
$\Delta P_{obl}$	axial pressure drop due to oblique flow
$\eta$	channel conversion efficiency
$\mu$	dynamic viscosity
$\nu$	kinematic viscosity, $\mu/\rho$
$\psi$	non-uniformity index
$\rho$	density
$d$	nozzle hydraulic diameter
$d_h$	channel hydraulic diameter
$f$	Fanning friction factor
$GHSV$	gas hourly space velocity
$k_c$	mass transfer coefficient
$L$	length of monolith
$\dot{m}$	mass flow rate
$N$	number of mesh elements
$\mathbf{P}_i$	porous inertial resistance tensor
$\mathbf{P}_v$	porous viscous resistance tensor
$Re$	inlet Reynolds number, $\rho U_{in} d / \mu$
$Re_c$	channel Reynolds number, $\rho u_c d_h / \mu$
$U$	mean axial velocity downstream of monolith
$u$	axial velocity
$u^*$	reference velocity, computed from wall law
$u_c$	channel velocity
$U_{in}$	inlet velocity
$V$	variance of prediction from experimental data
$v$	transverse velocity
$X^+$	non-dimensional distance along channel, $L/d_h Re_c$
$y$	distance from wall
$y^+$	non-dimensional distance from wall, $yu^*/\nu$